JOURNAL OF THE MECHANICAL BEHAVIOR OF BIOMEDICAL MATERIALS 28 (2013) 410–426

Available online at www.sciencedirect.com

ScienceDirect

www.elsevier.com/locate/jmbbm

Research Paper

A study of friction mechanisms between a surrogate skin (Lorica soft) and nonwoven fabrics ☆

*David J. Cottenden, Alan M. Cottenden**

Department Medical Physics & Bioengineering, University College London, Gower Street, London WC1E 6BT, UK

ARTICLE INFO

Article history:
Received 20 December 2012
Received in revised form
8 March 2013
Accepted 29 April 2013
Available online 15 May 2013

ABSTRACT

Hygiene products such as incontinence pads bring nonwoven fabrics into contact with users' skin, which can cause damage in various ways, including the nonwoven abrading the skin by friction. The aim of the work described here was to develop and use methods for understanding the origin of friction between nonwoven fabrics and skin by relating measured normal and friction forces to the nature and area of the contact (fibre footprint) between them. The method development work reported here used a skin surrogate (Lorica Soft) in place of skin for reproducibility. The work was primarily experimental in nature, and involved two separate approaches. In the first, a microscope with a shallow depth of field was used to determine the length of nonwoven fibre in contact with a facing surface as a function of pressure, from which the contact area could be inferred; and, in the second, friction between chosen nonwoven fabrics and Lorica Soft was measured at a variety of anatomically relevant pressures (0.25–32.1 kPa) and speeds (0.05–5 mm s^{-1}). Both techniques were extensively validated, and showed reproducibility of about 5% in length and force, respectively. Straightforward inspection of the data for Lorica Soft against the nonwovens showed that Amontons' law (with respect to load) was obeyed to high precision ($R^2 > 0.999$ in all cases), though there was the suggestion of sub-linearity at low loads. More detailed consideration of the friction traces suggested that two different friction mechanisms are important, and comparison with the contact data suggests tentatively that they may correspond to adhesion between two different populations of contacts, one "rough" and one "smooth". This additional insight is a good illustration of how these techniques may prove valuable in studying other, similar interfaces. In particular, they could be used to investigate interfaces between nonwovens and skin, which was the primary motivation for developing them.

1. Introduction

Most human skin spends much of its time in contact with fabrics, and mechanical interaction between the two is central to clothing comfort. There are also some contexts in which the health of skin is critically dependent on its interaction with fabrics, such as the facing materials of absorbent pads worn by incontinent people, or (bed)clothes between the body and load-

*Corresponding author. Tel.: +44 2072885670.
E-mail address: a.cottenden@ucl.ac.uk (A.M. Cottenden).

1751-6161/$ - see front matter © 2013 Elsevier Ltd. All rights reserved.
http://dx.doi.org/10.1016/j.jmbbm.2013.04.024

bearing surfaces of those susceptible to pressure sores. Yet the nature of friction between fabrics and skin is poorly understood, with the most fundamental experimental results still disputed; for example, there is no firm consensus as to the applicability of Amontons' law, or of the variation of friction with sliding speed, which must—in large measure—be attributed to a lack of robust, validated experimental methods. Furthermore, coefficients of friction are phenomenological. There is no widely recognised simple relationship between obvious surface properties and coefficients of friction for interfaces between either fabric (Ajayi, 1992; Hosseini Ravandi et al., 1994; Jeddi et al., 2003; Ramkumar and Roedel, 2003; Wang et al., 2006) or skin (El-Shimi, 1977; Nakajima and Narasaka, 1993; Bobjer and et al., 1993; Hendriks and Franklin, 2010) and other surfaces, despite the exertion of considerable experimental effort. The lack of a theory relating friction to material and surface properties denies guidance to the attempt to engineer materials with specified frictional properties.

If Amontons' law is to be rejected or placed on a firmer footing, much more must be understood about the mechanisms of friction in this instance: not only are the friction mechanisms far from clear, but the very nature of the interface is unknown. Accordingly, the work described in this paper set out to develop and validate two methods; the first, to measure the fibre footprint of nonwoven fabrics on surfaces; and the second to measure the friction forces between a surrogate skin and a selection of nonwoven materials of the kind commonly used in the body-facing coverstocks of incontinence pads accurately. Data generated using these two methods were then used to investigate the associated friction mechanisms.

2. Literature review

2.1. *Methods for measuring friction between (surrogate) skin and fabrics*

Methods reported in the literature for measuring friction between (surrogate) skin and fabrics can be divided into two main types: (1) rotational methods in which a circular pad or annulus faced with one material is pressed against the other material and rotated about its axis (Zhang and Mak, 1999); and (2) linear pull methods in which one material is simply translated across the other under load (Cottenden et al., 2008; Gerhardt et al., 2008, 2009; Derler et al., 2007; Gwosdow et al., 1986; Kenins, 1994; Hong et al., 2005; Comaish and Bottoms, 1971). Linear pull methods can be further divided into straight pull methods in which the translation is in a straight line across a flat surface (Cottenden et al., 2008; Gerhardt et al., 2008, 2009; Derler et al., 2007; Hong et al., 2005; Comaish and Bottoms, 1971) and curved pull methods in which a strip of one material is draped under load over a curved surface faced with the other material and is dragged along a curved path corresponding to a geodesic of the curved surface (Cottenden et al., 2008; Gwosdow et al., 1986; Kenins, 1994).

Each of these methods has its advantages and disadvantages. Rotational methods have the advantage that at least one commercial probe has been produced, lowering the barrier to beginning measurements. Such devices can also be self-contained and thus quite simple to use. However, they have several intrinsic limitations. The most fundamental is that since not all regions of the contact are experiencing equivalent conditions (sliding velocity is obviously proportional to radial distance) any reading must be an average, which cannot be interpreted without assuming some known variation of friction with velocity. These probes are thus by their nature not suited to fundamental measurements of how friction changes with velocity. Furthermore, strain fields and buckling patterns are often set up on compliant substrates, making the results hard to interpret with certainty.

Straight pull linear methods are the most direct of the three types of method, simply applying a load to an interface, putting it into sliding motion, and measuring the force required to initiate or maintain it. This has the advantage that the nominal condition of each part of the interface is the same, making the results easier to interpret. Due to the rectilinear pull the issues with buckling are generally less since the surface can move *en bloc* to accommodate, though for some interfaces problems still occur. The two main disadvantages of this type of method are that there is no known neat commercial implementation – thus requiring the equipment to be built in-house – and, more seriously, that it is difficult to provide a pulling force without either imparting a moment (due to the non-colinear pulling force and friction) or making the method very reliant upon perfect alignment of parts and non-robust against deformation.

Both rotational and straight pull linear methods suffer from difficulties with the shape of the probe on which the moving sheet material is mounted. It is well-known (though not universally appreciated) that a flat punch impressed into a compliant surface does not give rise to a uniform pressure distribution below it; rather, there are sharp peaks in pressure at the periphery (Johnson, 1985a). Though for interfaces that obey Amontons' law, departures from uniformity of pressure are clearly unimportant this is not so for more general interfaces. Further, frictional forces at an interface themselves distort the normal force distribution (Johnson, 1985b), quite apart from any incidental moments introduced by the equipment. These effects appear never to have been assessed or corrected for in friction measurements.

The curved pull linear method is the most indirect of the three methods, relying as it does upon the curvature of the surface to turn a tensile stress in the draped sheet into a normal stress which gives rise to friction. It is also an "integrated" method; that is, the measured force is the sum of a continuum of different contributions since the tension (and thus normal loading) change around the contact region. It is therefore necessary to use an established model to extract any desired interface parameters, and this will generally require some parameters of the curved surface to be known. In view of these points this type of method is not suitable for making fundamental friction measurements, though it is very suitable for certain routine measurements where a friction model has been established and one material is not usually flat, for example *in vivo* skin.

The novel method described and validated here aimed to overcome the majority of the problems exhibited by existing methods.

2.2. *Skin surrogates*

Any material co-opted as a surrogate skin must be equivalent to skin in the capacity in which it is being used. The overwhelming

majority of surrogate skins have been designed to be used to imitate the biological or histological properties of skin with little or no regard for their mechanical or textural similarity. They are designed to be stable for biological testing, but are not suitable for mechanical experiments. If there have been few mechanical surrogates, there have been fewer friction surrogates.

In their 2008 paper Gerhardt et al. (2008) stated that there was not at that time a sufficiently validated skin surrogate for friction against fabrics. In that work they referred to work undertaken by some of their group and published at a similar time (Derler et al., 2007) which compared friction between skin and a standard woollen fabric with that between a selection of proposed synthetic skin surrogates and the same fabric. This work (by Derler et al., 2007) gathered friction data for real skin by having subjects stroke a biaxial force plate faced with the test fabric, exerting varied normal forces; whereas most work on skin surrogates (using a reciprocating, faced circular punch) was at a single load. Comparison between the data for all of the skin surrogates and the skin itself showed that a synthetic leather composed of polyamide fleece with a polyurethane coating, Lorica Soft, was the closest match. They demonstrated that the coefficient of friction against the test fabric was similar to that of skin against the same fabric for normal loads from almost nothing to about 10 N. Additionally, Gerhardt et al. (2008) noted that the mean absolute deviation from the surface mean plane and a measure of the difference between the highest "peaks" and lowest "valleys" were similar for Lorica Soft and for young, dry, hairless skin.

2.3. *Friction mechanisms*

Based on the literature, there are a number of *a priori* likely nonwoven-skin (surrogate) friction mechanisms which are consistent with known experimental results for different pairs of surfaces, each mechanism with its own "signature" by which it would be revealed.

Plastic dissipation. The hallmark of plastic dissipation is the presence of persistent deformation to the contacting surfaces after sliding. This has been established not to occur for skin (El-Shimi, 1977; Nakajima and Narasaka, 1993), but there are no known negative results for nonwovens. Such deformation could in principle be easily detected in nonwovens by taking micrographs of a given region before and after an experiment. Plastic deformation is usually expected to lead to friction proportional to load.

Viscoelastic dissipation. It is very difficult to distinguish instantaneously between plastic and viscoelastic dissipation; the key difference is that viscoelastic deformation relaxes after an experiment, where plastic deformation does not. Viscoelastic deformation must therefore be observed by comparing any deformation during an experiment with that observed afterwards. Viscoelasticity can further be distinguished from simple non-dissipative elasticity by conducting experiments at different speeds: the former will vary with rate, while the latter will not. The variation of this type of friction with load depends on the details of the contact.

Pinning. "Pinning" refers to temporary trapping of features of one surface by those of the other. Although pinning in combination with pure elasticity does not produce friction, this mechanism can lead to relatively weak viscoelasticity causing a significant frictional force. This is because, although the dissipative effect of viscoelasticity may be weak at the mean sliding velocity, at time of slip contact points are travelling much faster than this, and so viscous dissipation is substantially increased. The key signature of this mechanism is fibres "pinging"; that is, suddenly freeing themselves from a pinning point and rapidly correcting. Merely observing pinging in an arbitrary system would not, of course, imply that this mechanism is relevant: in the absence of an internal or interfacial dissipative mechanism pinging conserves energy. However, skin is known to be viscoelastic, and thermoplastic polymers (such as constitute the fibres in common nonwoven coverstocks) are the prototypical viscoelastic materials, so observing pinging may reasonably be assumed to implicate pinning as at least *a* relevant mechanism. No characteristic variation of friction with load is associated with this mechanism.

Interfacial adhesion and dissipation. Friction due to true interfacial adhesion and dissipation is very hard to identify unambiguously due to a lack of visible mechanism. In practice, it must be inferred by assessing whether or not the other identified mechanisms account for the measured frictional behaviour. Adhesive friction varies linearly with contact area, though contact area's variation with load depends upon the nature of the surface.

The best approach, then, for identifying the mechanism(s) at play in a given system is to look for the corresponding diagnostic signs in the friction data; the materials before, during, and after friction experiments; and the nature and extent of the interface between the two material surfaces.

3. Strategy for the work, and structure of the paper

In order to establish which of the mechanisms identified in Section 2.3 (or indeed those as yet unidentified) are relevant at the nonwoven-skin (surrogate) interface of interest in the current work, the friction force and fibre footprint would ideally be measured simultaneously. Unfortunately, this proved impossible, but it was possible to gather all necessary data using only two distinct but linked experimental methods. The first involved using the shallow depth of field of a high magnification microscope to observe and measure the arrangement of the fibre footprint of nonwoven fabrics on a flat glass surface as a function of pressure. Being a rigid, transparent and readily available material with a flat surface, glass is much easier to work with than skin (surrogate) and – counterintuitively – it can be shown to be an informative

representative for both, allowing the contact area between tested nonwovens and skin (surrogate) to be calculated from the experimental results, up to an unknown multiplicative constant which depends on the skin relief. The method and corresponding results are described in Section 5, along with a justification for using glass.

Section 6 describes the second method and corresponding results. In this method, the friction force between nonwovens and skin surrogate was measured for a range of interfacial pressures and velocities while simultaneously observing the movement of fibres within the fabric using low magnification microscopy. The results from the two methods are considered together in Section 7 to identify the friction mechanisms operating. But first, the materials chosen for the work are described in Section 4.

4. Materials

The motivation for the work described here was to understand the interaction between human skin and nonwoven fabrics of the kind used in incontinence pads. However, skin is an awkward material to obtain and to work with; it is impossible to obtain identical samples and properties change rapidly with time *ex vivo*. Accordingly, a skin surrogate was used instead, for the purposes of method development. Lorica Soft (Ehrlich Lederhandels GmbH, Biberach, Germany; http://www.ehrlich-leder-lorica.de) was chosen as it is the only one that has been shown to mimic skins friction behaviour reasonably well (Section 2.2). It is supplied in a variety of colours and, arbitrarily, the white variant was chosen for the current work. In all force measurements the pulling direction was along the length of the roll.

A huge range of nonwoven fabrics is available but those based on polypropylene fibres are most commonly used for incontinence pad coverstocks (the layer that lays against the skin) and nonwovens experts at SCA Hygiene Products (part sponsors of this work) selected three of these for the current work (Table 1). All were experimental fabrics produced by a well-known supplier of nonwovens for the hygiene industry, and all had the same area density (basis weight in the language of textiles) of 17 g $m^{-2} = 1.7 \times 10^{-2}$ kg m^{-2}. Additionally, all fabrics had the same common surface treatments and the same thermal bonding pattern (calendering) in terms of the size, shape and lattice size of bonding points. They differed principally in the diameter of their fibres and in their fibre length per unit area of fabric, variables which were judged likely to be the principal factors in determining friction. Accordingly, the fabrics were chosen to represent as wide a range as possible of these variables. All samples of each nonwoven came from the same roll of the same batch; samples of each were thus as nearly equivalent as different samples of nonwoven ever can be. The method by which nonwovens are produced causes them to be anisotropic: the "upper" surface is different from the "lower" surface, and the "machine direction" is different from the "cross direction". There is no strict convention on which side of nonwoven coverstocks is in contact with skin in use, so the choice of which side to characterise is arbitrary, but must be consistent. The nonwovens used in this work were therefore labelled to identify their orientation.

5. Measuring the fibre footprint

The arrangement of fibres in nonwoven coverstocks is sparse: the fibres typically occupy much less than 10% of the nominal fabric volume and so when they lay against a surface, their actual contact area – the fibre footprint, through which any friction is mediated – with even a very compliant substrate is very much smaller than the nominal contact area. The method chosen to measure the fibre contact length made use of what is usually encountered as a limitation in optical microscopy: its limited depth of field (DoF). If the focal plane of the microscope is placed at the interface between a surface and a piece of nonwoven laying on it then any fibres that are not discernibly out of focus must be no further from the focal plane than a single characteristic depth of field distance. If the depth of field is shallow enough then this effect can be used to assess whether a fibre is in contact with the surface. From the contact length information it is quite simple to calculate contact area up to an unknown constant factor corresponding to the skin (surrogate) relief.

It would have been ideal to measure the fibre footprint of nonwovens against the Lorica Soft used in friction experiments but this proved impractical. Lorica Soft is opaque and so the interface would have to have been viewed through the nonwoven, but fibres "above" others at the interface obscure the latter sufficiently to make the resultant images very hard to interpret.

Additionally, because the surface of Lorica Soft is irregular, it is difficult to focus on the exact plane of the surface, even if the surface can indeed be reasonably approximated as a plane. Further, even if the Lorica Soft surface is "grossly" planar, like skin, it is covered in fine lines and wrinkles that by definition deviate from the plane: the DoF technique

Table 1 – A summary table for the nonwovens used in this project. The curious "decitex" unit used by textile technologists to measure linear density (*titre*) is defined as the mass in grams of 10 km of fibre. For these fibres this may be converted to a fibre diameter (that is, the length of fibre per area of fabric) using the circular cross section of the fibres and the density of polypropylene, $\rho_{PP} = 904$ kg $m^{-3} \pm 2$ kg m^{-3} (Kaye and Laby, 2004).

Fabric code	Linear density (dtex)	Fibre diameter (μm)	Fibre density (μm mm^{-2})
NW1	2.0	16.8±0.2	8.5×10^4
NW3	1.4	14.0±0.3	1.2×10^5
NW6	3.6	22.5±0.2	4.7×10^4

would unavoidably be inaccurate in this respect as it would consider the gross, planar surface not including these details. However, these limitations can be avoided if a smooth, flat, transparent glass surface is used instead of Lorica Soft, and the following section shows that, surprisingly, glass is an excellent surrogate for Lorica Soft (or real skin) for measuring the length of the fibre footprint.

5.1. *Justification for using glass to represent skin and Lorica Soft*

It is immediately apparent that the contact *area* between a nonwoven and glass will be radically different from that between the same nonwoven and Lorica Soft or skin under the same conditions. However, since the imaging method used in this work (described in Section 5.3) does not measure contact *area* but rather fibre contact *length*, the comparison that is really made is between the contact length for a nonwoven against glass or Lorica Soft/skin. The contact length of fibres is primarily determined by the mechanical properties of the fibre assembly which constitutes the nonwoven as the structure modulus for the nonwoven is substantially lower than the modulus of the fibre polymer or any of the facing materials. In view of this the idea that one substrate material can be substituted for another without significantly changing the contact length results no longer seems unlikely. This section demonstrates that – so far as contact length goes – nonwoven against glass is insignificantly different from nonwoven against Lorica Soft or skin. It is thus possible to calculate the contact area between fibre and skin/Lorica Soft (up to an unknown constant) from these nonwoven-glass contact length data and the material properties of skin/Lorica Soft.

If fibre segments are pressed against a surface there will be "bulging out" of the surface between the contacting fibre segments – to a degree dependent on the mechanical properties of the materials – which acts to bring additional fibre segments into contact with the surface, causing rearrangement of all fibres and a second order change in the fibre footprint. If the bulge heights for all compared materials are small relative to a fibre diameter then bulging has no significant effect on contact length for any material, leaving contact length determined entirely by the properties of the nonwoven and independent of those of the substrate. To ascertain whether glass can be used to represent skin and Lorica Soft in such measurements, it is necessary to obtain and compare the characteristic "bulge" heights of the surfaces. Given the small deformations involved and the difficulties of measuring them directly, the problem of calculating bulge heights was addressed using linear elasticity theory in a half space. The complexity and variety of the fibre contact segments precludes any attempt to model the details directly; instead, noting that most fibres have a low curvature it is more helpful to consider the behaviour of an ensemble of straight fibres of known pitch and dimensions.

In order to obtain a solution with finite near and far fields, the support for contact force density must also be finite. In the interests of simplicity, it is assumed here that a constant force density p is exerted over the interval $[-L, L]$ in x and $[-a, a]$ in y, with $2a$ corresponding to contact width and $2L$ a typical fibre contact length. From these assumptions the surface deflection can be calculated using Boussinesq's solution (see Johnson, 1985c):

$$u_z(x,y) = p\frac{1-\nu^2}{\pi E}\int_{-a}^{a}\int_{-L}^{L}\frac{1}{\sqrt{(y-y')^2+(x-x')^2}}\,dx'\,dy'$$

$$= p\frac{1-\nu^2}{\pi E}\int_{-a}^{a}\log\left(\frac{\sqrt{(y-y')^2+(x+L)^2}+(x+L)}{\sqrt{(y-y')^2+(x-L)^2}+(x-L)}\right)dy'$$

$$= p\frac{1-\nu^2}{\pi E}\begin{pmatrix} f(y+a,x+L,x-L)-f(y-a,x+L,x-L)\\ +f(x+L,y+a,y-a)-f(x-L,y+a,y-a)\end{pmatrix},$$

where

$$f(\alpha,\beta,\gamma) := \alpha\log\left(\frac{\sqrt{\alpha^2+\beta^2}+\beta}{\sqrt{\alpha^2+\gamma^2}+\gamma}\right),$$

E is Young's modulus and ν is Poisson's ratio. The original question of the characteristic "bulge" between fibres can now be addressed by taking multiple instances of this solution centred on locations separated by λ and adding them together. An example of the results obtained is shown for reference in Fig. 1; the family of curves represents surface deflection as a function of distance from the central fibre's axis for a variety of values of $\Pi = p_{nom}(1-\nu^2)/E$. The maximum "bulge" height for fibre contact segments with the typical parameters used in the graph is tabulated in Table 2 for a variety of Π values.

Before any characteristics can be obtained, the parameters of the model (a, L, characteristic distance between fibres (λ), and p) must be related to known quantities. For L and λ this is easily done: results presented later (Section 5.5) show that the mean fibre contact length varies very slowly with pressure and is typically about 400 μm, and that if the fibre contacts were laid out in parallel and equally spaced straight lines then they would be separated by about the same distance. Contact pressure can also be dealt with: taking the assumption of uniformity, $p = p_{nom}\lambda/2a$ where p_{nom} is the nominal pressure. Contact width is most convincingly estimated by making use of the two-dimensional Hertz theory for an

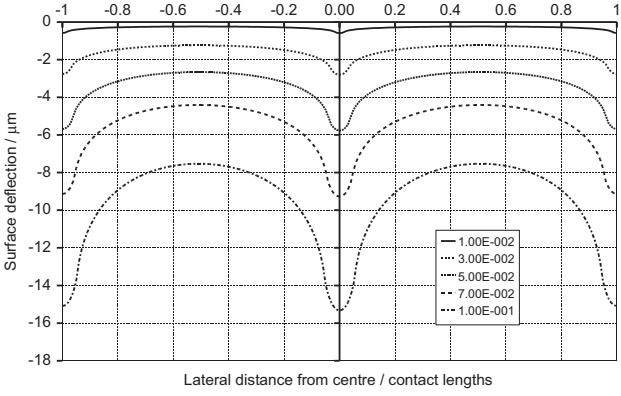

Fig. 1 – Surface deflection due to parallel, aligned fibre segments of length 400 μm each separated by 400 μmm, typical values for the nonwovens used in this work. The curves each represent a different pressure (material independent – Π values given in the key). For comparison, the fibre diameter is taken as 20 μm. For simplicity only five fibres were used to create this graph, but as deflections rapidly decay very little error is introduced.

Table 2 – Bulge height calculated on the basis of five fibres aligned as described in the text. The "pressure" is in fact $\Pi = p_{nom}(1-\nu^2)/E$ in order to make the table material-independent, where p_{nom} is the nominal applied force per unit area, ν is Poisson's ratio, and E is Young's modulus.

Pressure (Π)	Maximum deflection (μm)	Minimum deflection (μm)	"Bulge height (μm)
1×10^{-3}	2.2×10^{-2}	7.5×10^{-3}	1.4×10^{-2}
1×10^{-2}	5.9×10^{-1}	2.4×10^{-1}	3.5×10^{-1}
3×10^{-2}	2.8	1.2	1.6
5×10^{-2}	5.8	2.7	3.1
7×10^{-2}	9.3	4.4	4.9
1×10^{-1}	15	7.5	7.8

infinite cylinder pressed into an elastic half space. For this system, the contact width is given by

$$a = \sqrt{\frac{4PR}{\pi E^*}}, \tag{1}$$

where P is the linear force density, R is the cylinder radius (set to 10 μm in the following analysis – see Table 1), and (for a rigid fibre) $E^* = E/(1-\nu^2)$ is the plane modulus (Johnson, 1985d). Linear force density is related to mean pressure by $P = 2pa = p_{nom}\lambda$ (Johnson, 1985d), so

$$a = \sqrt{\frac{4p_{nom}\lambda R}{\pi E^*}} = \sqrt{\frac{4\lambda R}{\pi}\Pi}. \tag{2}$$

The results presented in Fig. 1 and Table 2 suggest that – provided $\Pi < 5 \times 10^{-2}$ – the bulge is sufficiently small that few "additional" fibre contacts will be formed; that is, moving between two substrate materials for which Π obeys this condition is unlikely to cause any substantial alteration in the fibre contacts.

For micron-scale indentations the relevant mechanical properties for skin are those of the stratum corneum (SC). The reported modulus of the SC varies widely, but at 100% RH (most compliant) the lowest result known is $E^* = 6$ MPa Park and Baddiel, 1972, giving $\Pi = 8 \times 10^{-3}$ for the highest loads used in this work. (A review of the mechanical properties of SC is provided by Cottenden, 2011). As part of the present work the stiffness of the laminar structure of the Lorica Soft was measured in uniform stress (compression, normal to the sheet) and uniform strain (tensile, parallel to the sheet), and the most superficial lamina was found to have a stiffness, $E^* > E^*_{unif\ strain} \approx 6$ MPa for $\Pi = 8 \times 10^{-3}$ again. At $\Pi = 8 \times 10^{-3}$ the bulge height is 0.3 μm, which is 1%–2% of a fibre diameter. It is thus reasonable to expect that second-order fibre rearrangement will be equally negligible against skin or Lorica Soft as against glass (where Π is substantially smaller).

In summary, although contact length measurements cannot be taken on skin and Lorica Soft (as would be ideal), measurements made on glass are excellent surrogates.

5.2. *Apparatus*

The apparatus designed to gather DoF data is very simple; it need only apply known pressures within the confined space of the microscope stage, so consists of two perspex plates and an arrangement of springs (Fig. 2). The springs are above the upper plate and serve to apply a compressive force. As the wing nuts are tightened, the vertical travel – and so the force they apply – can be controlled very precisely. The pressure plates apply their pressure to a piece of nonwoven held between a pair of crossed microscope slides (chosen for transparency and flatness; $24.5 \pm \frac{1}{4}$ mm × $76.0 \pm \frac{1}{4}$ mm). The high stiffness of glass compared to the applied pressures ($E_{glass} \approx 80$ GPa (Kaye and Laby, 2004), $p_{max} = 50$ kPa) means that no significant deformation of the slides will occur, and thus flat "anvils" can be safely used (see Section 6.1). Experiments were conducted using five different pressures spanning the range selected for pulling experiments (see Section 6.1). Due to the difficulty in assessing when the springs first apply pressure to better than about 0.5–1 rotation, the very lowest pressures (0.5 kPa and 1.5 kPa) were achieved using pure deadweight loading, omitting the upper plate and adding a small additional weight with a hole (for microscopy) on the top. This simple system works well for low pressures, but the size of the required deadweight and the consequent instability that would be suffered make it inappropriate for higher pressures (5 kPa, 15 kPa, and 50 kPa).

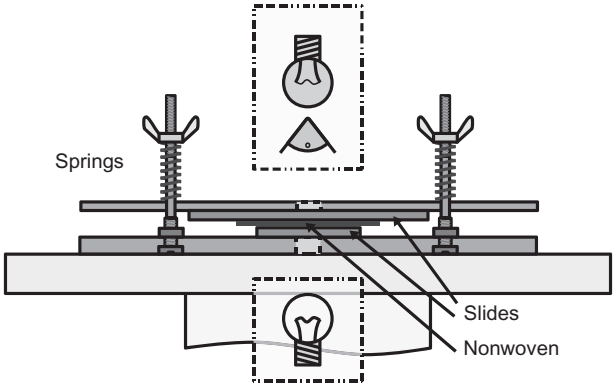

Fig. 2 – Simple apparatus used to apply pressures to nonwoven under a microscope. The upper and lower surfaces are drilled so that there is an entirely uninterrupted light path from the light source to the immediate environment of the nonwoven, and from there to the microscope lens. The slides and nonwoven are not attached to the rest of the assembly and can be freely positioned.

5.3. *Method for raw data collection*

The method for measuring fibre contact lengths can be divided into two main stages: gathering raw micrographs;

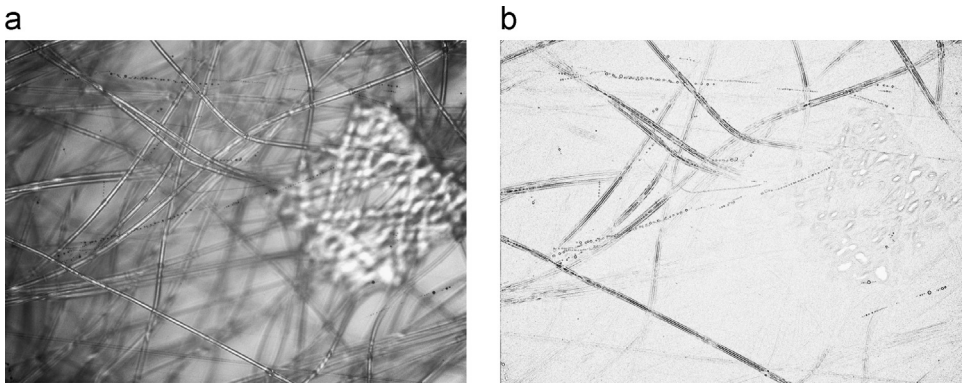

Fig. 3 – An example of DoF microscopy. (a) Reflection micrograph of the side of a NW1 sample *closer* to the microscope pressed against glass (an *upper interface*) at 5 kPa using a ×10 lens. It is clear that some fibres are focused and others are not. (b) The same image filtered to enhance sharp edges; the focused fibres are now much more apparent.

and processing those micrographs into distances. To gather raw micrographs, nonwoven samples were cut (30 mm square) and marked for orientation (machine direction and lower/uppermost surface in production). Preliminary experiments showed that nonwoven samples behave "plastically" within the pressure range used here; that is, contact images taken at a low pressure before and after subjecting the sample to a nominal 50 kPa pressure showed significant differences, even to the eye. This problem was avoided by using each nonwoven sample only once before discarding it. Note that this plastic deformation is quite distinct from the plastic junction formation already referred to as a possible friction mechanism. Three repeats were run for each of the three nonwovens at each pressure, giving a total of 45 experiments. Micrographs were gathered using a DMLM microscope and DFC 320 (both Leica Microsystems (UK) Ltd., Milton Keynes, UK) and QWin software (version 3.2.0, Leica Microsystems (UK) Ltd.). The QWin "Mosaic" facility (for gathering multiple images and splicing them together) was used to enable micrographs of large areas of nonwoven (approximately 5 mm square) to be obtained. Images were gathered in reflection mode so as to reduce variation in lighting that the "upper" nonwoven surface would suffer by virtue of the fibres beneath. In consequence, it was necessary to use shading correction to ameliorate the otherwise marked darkening of off-axis image pixels; the procedure for this is described in the QWin documentation.

5.4. *Method for processing raw data*

Depth of field (or at least its appearance) depends upon many parameters including illumination and magnification, but also the more subjective issue of when a feature is deemed to have become unfocused, which is difficult to judge directly by eye. An image of NW1 against glass is shown in Fig. 3a to illustrate the images that can be acquired but, although the distinction between focused and unfocused fibres can be discerned, it is not very clear. In consequence, it is helpful to enhance the raw images, which is done by considering the green channel of the RGB image and taking the modulus of the gradient. The gradient picks out the sharp changes which are characteristic of focused features and suppresses the blurred features that clutter the raw images; an enhanced version of Fig. 3a is shown in Fig. 3b.

Although the contact fibre segments shown in Fig. 3 are fairly clear to the human eye (especially when seen in conjunction with the original image), to a computer the task of identifying contact fibre segments is formidable. Accordingly, a semi-automated approach for identifying and measuring fibre contacts was adopted. The approach was to print out the enhanced raw images, manually trace them onto acetate sheet, scan these back into the computer, and then use readily available software to convert the uniformly coloured lines on a blank background into Bézier curves. Scanned images were initially processed using Gwenview (version 2.3.2, http://www.gwenview.sourceforge.net) to crop off the labelling and other uninformative regions and convert the image to bitmap format. The bitmap was then transferred to the GNU Image Manipulation Program (the GIMP, version 2.6.7, http://www.gimp.org), where the colour curves were adjusted to a step function (transition at 50% intensity) to suppress grey noise and reduce intensity variation in the lines. Additionally, artefacts such as dust on the scanner glass and smudges on the acetate were removed at this stage. The "cleaned" bitmap was then saved and passed to a BASH script which ran an open source bitmap tracer (Auto Trace, version 0.31.1, http://www.autotrace.sourceforge.net) to extract Bézier curves, followed by a purpose-written programme which extracted curve lengths and mean curva tures from the Bézier curves. Having passed through this process the data were in a form in which they could readily be interrogated.

5.5. *Results and analysis*

The data from each micrograph can be represented as a single point on a graph of contact length against pressure. Fig. 4 shows an example graph for NW1, showing three repeats at each of the five pressures. Two features of these "raw" graphs are particularly interesting. First, at a given pressure the spread of contact lengths is much larger than can be attributed to the error in the technique (indicated by the error bars). This implies that it is principally due to

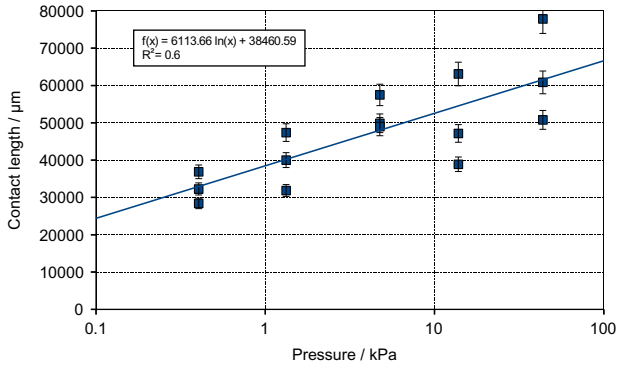

Fig. 4 – Contact length against pressure for NW1 and glass. Each point corresponds to a single micrograph. In all cases the pressure error bars are smaller than the marker; contact length error bars are based upon the *approximate* ±5% total process error identified in method validation work.

material variation. The second observation is the very slow (approximately logarithmic) increase of contact length with pressure: a pressure increase of two orders of magnitude leads to less than a factor of three increase in contact length in all cases. This is very surprising.

The surfaces of real interest are skin (surrogates) and – unlike glass microscope slides – they exhibit surface relief. In order to obtain an accurate assessment of the true contact lengths for such surfaces this must be taken into account. This might be done by measuring the relief of the skin (surrogate) and producing a statistical description of the proportion of the surface that is "at the top". The measured contact length would then be normalised to this and analysis of the corrected values would proceed. In other words, all of the nonwovens would be normalised in the same way for a given surface, and (following from the indentation analysis in Section 5.1) the normalisation would not vary with load. In consequence, neither the variation of length with load nor the comparisons between the nonwovens would appear any differently whether the lengths were corrected or not, other than by a change of scale. It was therefore concluded that such a time-consuming and only mildly beneficial project should not be undertaken at this stage.

The principal shortcoming of the new experimental data is that they relate to contact length rather than contact area. No effective means of measuring contact width has been found, but by making some assumptions it is possible to infer the contact width and thus area from the length data already gathered. To do this, the same simple model can be used as was reported in Section 5.1, where it was used to estimate bulge height. However, whereas there (for simplicity) the contact length was assumed constant, here it is allowed to vary according to the logarithmic form observed.

Referring to Eq. (2) and observing that $\lambda = 1/\hat{l}$, where $\hat{l}$ is the contact length normalised to sampled area,

$$a = \sqrt{\frac{4R}{\pi E^*}\frac{p_{\mathrm{nom}}}{\hat{l}}}.$$

Since all of the contact length against pressure graphs are well-fit by $\hat{l} = \delta \log(p_{nom}) + \epsilon$ this can be written as

$$a = \sqrt{\frac{4R}{\pi E^*}\frac{p_{\mathrm{nom}}}{\delta \log(p_{\mathrm{nom}}) + \epsilon}}. \tag{3}$$

As the two most commonly advocated models of skin-X friction are adhesion and "viscoelastic ploughing", it is interesting to predict the variation of contact fraction (proportional to adhesion) and a representative quantity for viscoelastic dissipation as functions of pressure. Considering first contact fraction, it is clear that by use of Eq. (3)

$$\phi := \frac{A_{\mathrm{true}}}{A_{\mathrm{nom}}} = 2a\hat{l} = \sqrt{\frac{16R}{\pi E^*}}\sqrt{p_{\mathrm{nom}}\hat{l}}.$$

Again, using the logarithmic fit to the experimental curves this becomes

$$\phi = \sqrt{\frac{16R}{\pi E^*}}\sqrt{p_{\mathrm{nom}}\{\delta \log(p_{\mathrm{nom}}) + \epsilon\}}.$$

In principle all of the quantities in this equation are determinable or known, but in practice the reduced modulus for the stratum corneum is poorly known and very dependent upon ambient relative humidity. Fortunately, this merely represents a scaling factor, so although the graph in Fig. 5 (and similar ones for the other nonwovens) have assumed a reasonable value of 500 MPa (Park and Baddiel, 1972) the form of the graph is not dependent on this value; the form equally applies to Lorica Soft. The relief effect equally represents an unknown scaling. The graphs themselves are very interesting, both individually and in comparison with each other. All are similar in form; a power law fit is good in all cases, with an exponent in the range of 0.57–0.61. It is also informative to compare this to the behaviour that would be predicted for a single long fibre under load, where Eq. (1) shows a square root dependence of a (and thus $2aL$) on pressure. In moving from that simple system to the one at hand, the increase of contact length with nominal pressure causes line loading to increase sub-linearly with nominal pressure (acting to slow the increase of contact area) but itself directly acts to increase contact area; apparently the latter effect dominates.

Comparison between fabrics is fraught with uncertainty because the visibilities and depths of field of the fibres are not identical, but is nonetheless interesting, if limited. The three

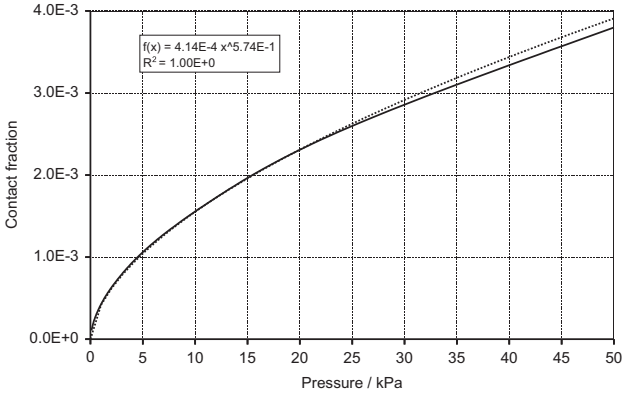

Fig. 5 – Contact fraction, ϕ, for NW1, as predicted from the assumption of Hertzian contact and the measured relationship between nominal pressure and contact length. The solid line is the prediction; the broken line is the power law fit.

graphs are very similar; no clear distinction can be seen between NW3 and NW6, while NW1 gives rise to perhaps 20% larger contact fractions. Since NW3 and NW6 have fibre diameters which differ by a factor of 1.6 this is interesting by itself; given the substantial difference between their respective contact lengths, it must be concluded that the flatter and wider contact of a larger diameter fibre roughly compensates. The larger contact fraction of NW1 appears to stem from it also having the largest contact length. This suggests that contact length is the more significant factor.

Regarding viscoelastic ploughing, there is little consensus in the literature as to the details of its origins, and the most coherent models are complicated. It would be difficult – and of doubtful utility – to apply any model in detail to the measured fibre contacts, but rather more sensible to deal with averaged quantities. Accordingly, a very simple model after the original approach of Greenwood and Tabor (1958) is used. Its shortcomings (such as using Hertzian contact mechanics in the presence of friction and of rate-dependent stiffness) are recognised, but given the small deformations and approximate nature of the application they are more than matched by the simplicity it offers.

Following the spirit of that model, the horizontal forces exerted on the front of a Hertzian impressed cylinder are calculated; the force considered as energy per unit distance, and the fact that γ of the energy is never regained at the back recalled; and the friction force thus given as γ times the "front" force. In this context it is more sensible to work with applied normal force per unit length, $\hat{f}$, and to assume an infinitely long cylinder for the purposes of calculations. Referring to Fig. 6,

$$d\hat{f} = p \sin\theta R \, d\theta,$$

where p is contact pressure, θ is the angle from vertical, and R is the cylinder radius. For Hertzian contact $p = (2P/\pi a)\sqrt{1-r^2/a^2}$ (Johnson, 1985d), where $r = R\sin\theta$ is the distance from the centre, a is the limit of contact, and P is the line loading, and as argued in Section 5.1, obeys $P = p_{nom}/\hat{l}$. Substituting this distribution in and solving, the friction force per unit length is

$$\hat{f}_{fric} = \gamma \frac{2Pa}{3\pi R}.$$

This must now be moved from the situation of a single infinite cylinder to the collection of finite fibres that in fact occur. However, since introducing variation in orientation will merely give rise to a geometric prefactor of order unity for the price of considerable work, and the loss factor γ and the scaling effect of relief are in any case unknown, it will be assumed for simplicity that all fibres are broadside on to the direction of motion. As this is the case, subject to the assumption of uniformity of pressure along the length of the contact it follows that friction force per unit area is simply

$$\hat{f}_f = \gamma \hat{l} \frac{2Pa}{3\pi R} = \gamma \frac{2p_{nom}a}{3\pi R}.$$

Substituting for a using the expression in Eq. (3),

$$\hat{f}_f = \gamma \frac{2p_{nom}}{3\pi R}\sqrt{\frac{4R}{\pi E^*}\frac{p_{nom}}{\delta \log(p_{nom}) + \epsilon}} = \gamma\sqrt{\frac{16}{9\pi^3 R E^*}\frac{p_{nom}^3}{\delta \log(p_{nom}) + \epsilon}}. \quad (4)$$

Fig. 7 shows an example plot for NW1 of Eq. (4) for the same material parameters used before, and for $\gamma = 0.5$; the choice of γ merely scales the result. It should be noted that

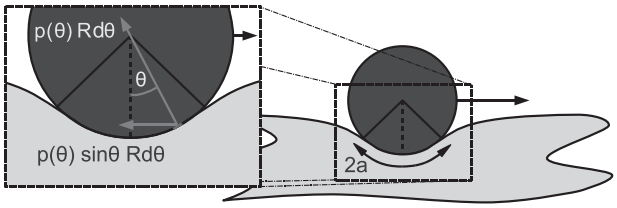

Fig. 6 – The horizontal force per unit length of fibre can be found by considering the horizontal component of the Hertzian pressure.

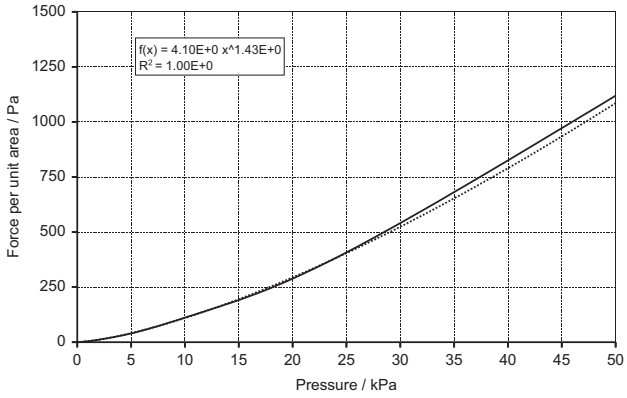

Fig. 7 – Prediction for the form of viscoelastic dissipative forces for NW1 following the spirit of Greenwood and Tabor (1958), assuming Hertzian contact and using the contact length against pressure relationship observed experimentally. The solid line is the prediction; the broken line is the power law fit.

these results are not quantitative predictions of the magnitude of viscoelastic force in friction testing against the skin; they are indications of the rough form that it would be expected to take if simple viscoelasticity were important. Again, the graphs are well-fit by power laws, with exponents varying in the range 1.38–1.43. Reiterating the caveats about comparisons between nonwovens, it is nonetheless unsurprising that again NW3 and NW6 behave very similarly, and (because of the form of the function) NW1 falls beneath them. Little more can be said about these graphs at this stage.

Comparing the two effects, it is interesting to note that the exponents in the power law relationships predicted for contact fraction (relating to adhesion) and viscoelastic dissipation are very different, around 0.6 and 1.4, respectively. In particular, coefficients of friction dominated by each would have qualitatively very dissimilar behaviour at low pressure, with the former diverging and the latter moving smoothly to zero. Comparison of friction results with these results is made in Section 7.

6. Force against displacement and low magnification microscopy

6.1. *Apparatus*

The apparatus for this experiment was designed to deliver uniform stress over the nonwoven-Lorica Soft interface

whilst driving it at a constant speed. Simultaneously, the force required to maintain motion, and the behaviour of the Lorica Soft and the nonwoven fibres needed to be observable. These requirements were all met by the apparatus illustrated in Fig. 8. At the heart of the equipment is a slider mounted with two rectangles of Lorica Soft (100 mm long (in the direction of motion) and 50 mm wide) – one above, one below – against which transparent, nonwoven-covered anvils are held and loads applied using dead weights. The use of two nonwoven-Lorica Soft interfaces was to avoid the turning moment that would have been encountered with one if the line of pull of the tensometer had not passed exactly through the nonwoven/Lorica Soft interface. The 26 mm diameter anvils (each identified with a lower case Greek letter – see Table 3) were made of epoxy resin, and shaped so that the normal and transverse force densities were constant. This required a separate set of anvils for each pressure and material used; the method for making anvils is described in the appendix. Nonwoven was fixed to the anvils at the periphery using nail varnish, and Lorica Soft to 2 mm thick perspex on either side of the slider using epoxy resin. The slider assembly was pulled between the anvils at a constant speed by a tensometer (MTT170, Diastron, Andover, UK) which measured the force required to maintain motion. By virtue of the transparency of the anvils and relatively sparse nature of the nonwoven it was possible to observe the fibres in the nonwoven and some of the Lorica Soft surface using a microscope and camera (Leica DMLM and DFC295, Leica Microsystems (UK) Ltd., Milton Keynes, UK); a micrographic video of sliding was recorded for later evaluation using the LAS software for the microscope camera.

All experiments were carried out in an environmentally controlled room held at 23 °C±1 °C and 50%±5% relative humidity in which materials were stored for at least one hour prior to testing.

All experiments were carried out at one of five different velocities ((0.05 mm s^{-1}, 0.167 mm s^{-1}, 0.5 mm s^{-1}, 1.67 mm s^{-1}, and 5 mm s^{-1}) covering the range of the tensometer, and five different loads (pressures) (0.25 N (0.56 kPa), 0.73 N (1.5 kPa), 2.65 N (5.0 kPa), 8.09 N (15 kPa) and 19.01 N (32.1 kPa)) covering the physiologically relevant range (Ferguson-Pell et al., 1976).

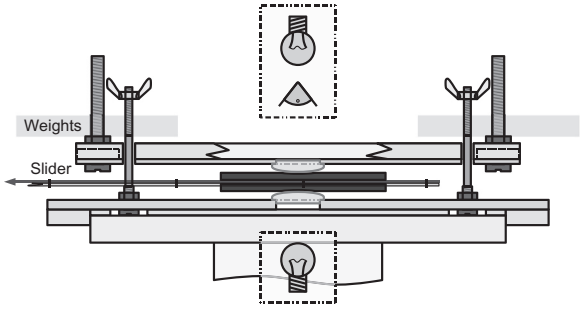

Fig. 8 – The apparatus for force and low magnification microscopy experiments. The upper surface slides freely on the rods, providing the pressure, but is fairly unconstrained in terms of orientation to enable it to adjust to any imperfections in the anvils. The anvils are faced with nonwoven (not shown) and are pressed against the slider assembly which bears the skin (surrogate). The whole assembly is shown mounted on the microscope stage for which it was designed.

To clarify the following description, some terminology must be introduced. The procedure in which the tensometer shuttles back and forth with the slider once is referred to as a *cycle*; a pre-programmed set of cycles is referred to as a *phase*; a set of phases designed to constitute a test of a particular combination of parameters and materials (for example, a chosen slider and nonwoven combination at a fixed speed) are referred to as a *run*. It is, of course, possible for a phase to consist of only one cycle, and a run to contain only one phase.

In general, a first phase of experiments with a nonwoven sample consisted of ten cycles – materials wore quite rapidly initially – with subsequent phases consisting of five cycles. The only exceptions to this were experiments at the slowest speed where only those cycles deemed strictly necessary were undertaken in order to save time. A given run continued until the majority of cycles in a five cycle phase were consistent; that is, they showed acceptably small random variation, and no longer any tendency for the force–displacement trace to drift up or down. In consequence mean traces – calculated as simple point-by-point arithmetic means – were usually based on four or five individual cycles, with three quite common and two very rare. Two different Lorica Soft sliders were used, both cut in the same orientation but from different edges of the material roll and from different ends of the sample; these were designated sliders L8 and L11. Nonwovens were arbitrarily considered in the order NW6, NW3, NW1.

In this work the initial wear-in period was not studied. This was not because it was judged unimportant, but rather because the long-term behaviour is also important and is less awkward to measure. Further, it is reasonable (though certainly unproven) to think that the same mechanisms will act as in the long-term case, though on an unworn nonwoven fibre configuration. Studying the initial friction behaviour and checking this hypothesis would be interesting, but is not done here.

6.2. Results

The results for this experiment divide fundamentally into force data and microscopy data. An example of raw (individual cycle) data is given in Fig. 9, from which it is apparent that there is a "wear-in" period of around 12 cycles during which the friction force gradually diminishes to a relatively repeatable trace. These raw graphs give rise to mean-trace graphs, produced by averaging data for all cycles beyond the "wear in" period. To facilitate simple comparison between curves all friction forces were normalised by the mean load on the two anvils for a given run. Traces showing variation with velocity are given in Fig. 10, and graphs summarising the variation of the trace with load are shown in Fig. 11. Since the slight difference in load between the two anvil faces complicates matters slightly, traces grouped by load are labelled with the letter designations of the anvils used. It is immediately apparent that whilst in most cases there is very considerable similarity between the traces for a given slider

Table 3 – A summary of anvils produced. Pressure and load are not proportional as the contact area varied with load.

Designation	Pressure (kPa)	Load (N)
ρ	32.1	19.0
σ	1.5	0.73
τ	5.0	2.65
ϕ	0.6	0.25
χ	15.0	8.09
ψ	6.3	3.14
ω	2.4	1.23

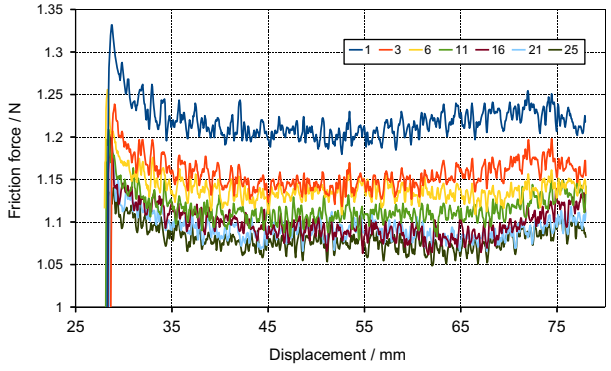

Fig. 9 – An example of a new slider (L11) "wearing in" over 25 cycles. This experiment used the τ–ψ combination of anvils, NW6, and a sliding speed of 1.67 mm s^{-1}. The final five cycles (21–25; only 21 and 25 shown) can be clearly seen to have converged and the run-to-run force reading to have stabilised.

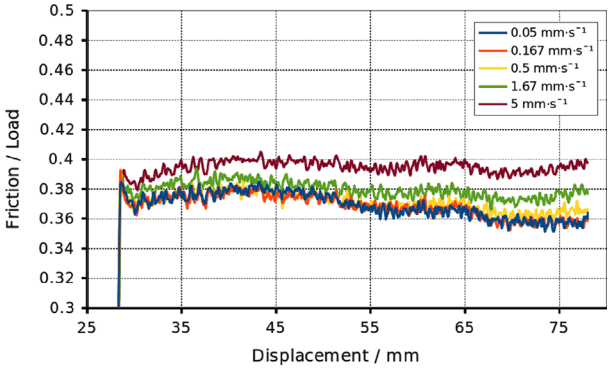

Fig. 10 – Comparison of normalised force–displacement curves at different sliding speeds for NW6 and the L8 Lorica Soft slider with anvils τ and ψ.

against different nonwovens, traces for the two sliders against the same nonwoven often differ markedly. This is not unexpected: it is simply a reflection of the inhomogeneity of the Lorica Soft, and in fact provides a means by which to assess variation with sliding speed and load independently of the shape of the force–displacement curve.

Microscopy data from this experiment were very disappointing. Due to the very limited reflection from the Lorica Soft surfaces (skin could be expected to be similar) the contrast in the fibres was poor, and they had very limited

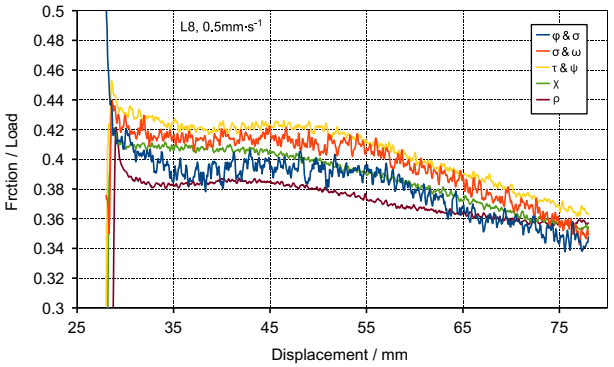

Fig. 11 – Comparison of normalised force–displacement curves at different loads (different anvils) for NW3 and the L8 Lorica Soft slider at 0.5 mm s^{-1}. The traces are labelled by the designation of the anvils used to take the measurements: the differential in load between the two surfaces precludes labelling them with a simple pressure, so this simple expedient has been adopted here and henceforth.

visibility against the mottled backgrounds. The only general comment that can be made is that the fibres of all fabrics were seen to move in essentially all circumstances. Some also periodically "flashed"; that is, they briefly reflected light before appearing dull again. It is conjectured that this behaviour is due to the fibres being lifted up off the surface, thus changing their optical properties. However, "pinging" – that is, movement with the slider followed by rapid correction – was not seen. Nevertheless, whatever their other shortcomings the constant focus of the videos corresponding to sliders L8 and L11 made it clear that the slider thicknesses were constant to less than 100 μm, which suggests that systematic noise due to non-constant thickness will have been no more than a few millinewtons and can thus be ignored.

6.3. *Analysis*

Considering the data as a body, it is apparent that (a) the relative scale of the short-wavelength variation on the force–displacement traces decreases with increasing load; (b) in general, friction increases with velocity, though not very much; (c) in several cases the first short distance of a trace does not conform to the patterns that the remainder does; and (d) in almost all cases the traces for a given slider share a strong family resemblance; that is, their shapes are discernibly alike. These observations are valuable guides to quantitative analysis.

In quantitative terms, the relationship between friction force and load, and friction force and sliding speed for the Lorica Soft data are the simplest to establish. Considering friction force against load, it is useful to extract a single number from the friction trace so that a plot of friction force against load can be constructed. In all cases the traces are not uniform horizontal lines, so some interpretation is required in order to extract such a characteristic. Fortunately, as noted it is apparent that in the majority of cases the traces for different loads applied to the same interface are not far from

being mathematically similar; that is, when scaled they can be approximately superimposed; a more detailed discussion of this is given below. This means that, since the relative magnitude of the curves is of much more interest than the absolute values, any linear magnitude characteristic can be used for comparison. The chosen characteristic is (unnormalised) mean friction force over the interval 40–78 mm: this excludes the sometimes atypical initial section of the traces but makes use of all of the remainder. This is plotted against the mean of the loads on the two anvils; for these purposes the difference in loads on either anvil was taken as the mean load due to the slider's weight over the interval 40–78 mm from the start of travel.

Fig. 12 shows friction force against load (both calculated as discussed) for NW1 and both sliders. In each NW1 case – and also for NW3 and NW6 – a straight line fits the data with a coefficient of determination (R^2) of 0.999 *or higher*. Having established good agreement between a linear fit and the data, coefficients of dynamic friction, μ, can be meaningfully calculated (recalling that the measured friction is the sum of that from two interfaces). Considering graphs of point-wise calculated μ against load (an example is given in Fig. 13) it is clear that there is no coherent systematic variation of μ with load: the apparent positive correlation of coefficient of friction and load NW6-L11 stands against the negative correlation for NW6-L8. In view of this, so far as variation with normal force goes, the Lorica Soft-nonwoven system obeys Amontons' law to very high precision for the nonwovens considered here.

In spite of this excellent agreement it is nonetheless interesting to note that a better fit can be achieved at low loads by using a power law fit (index typically 0.98) rather than a linear fit; an example of such a fit is shown in Fig. 12. In many cases this actually decreases the coefficient of determination (never below 0.999) because the same absolute deviation at low loads gives rise to the same absolute residual as at higher loads even though in absolute terms the conditions are more stringent at low loads. From the perspective of improving low-load agreement, the reduction in coefficient of determination means little. In favour of the power law fit is the fact that the error bars at low loads mandate a much closer agreement between data and fit than a linear fit can achieve; a power law fit passes within

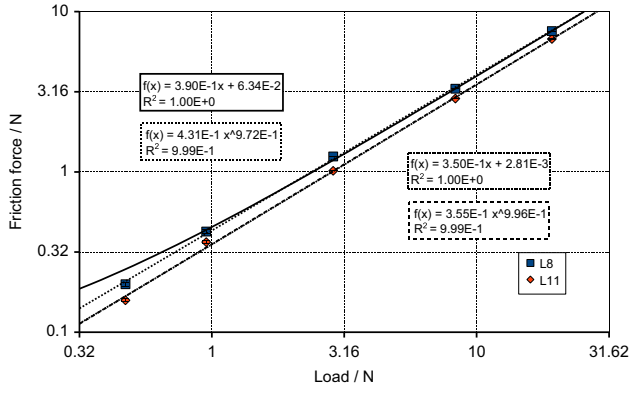

Fig. 12 – An example summary plot of friction force against load for NW1 against each Lorica Soft slider.

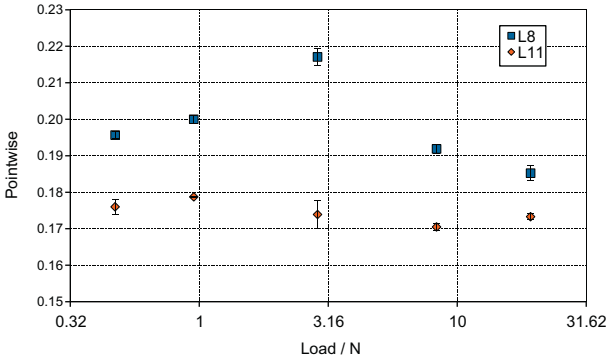

Fig. 13 – An example summary plot of pointwise calculated coefficients of friction against load for NW3 against each Lorica Soft slider.

most of the error bars on most graphs, whilst a linear fit frequently does not. This could be for two reasons: (1) this is the fundamental manner in which the interface behaves; or (2) a confounding factor that varies nonlinearly with load is complicating matters. It is impossible to distinguish between the two based on these data, but as the difference is very slight this does not present a practical problem for the remainder of the analysis.

All the preceding discussion relates to dynamic friction; static friction has not been considered. This is because of the already observed fact that the early portions of friction–displacement curves are not terribly reproducible. It would thus be impossible to perform an analysis in any depth on static friction; and in simple terms the initial portion of curves is broadly in proportion with the latter portions, so general statements about dynamic friction apply in good measure to static. It should be noted that the one clear pattern for the initial portions of friction–displacement curves – that the trace rises to higher loads and falls to lower ones – is simply a consequence of approximately the same force being used to set the equipment in the first place: it was higher than the smaller dynamic friction forces and lower than the higher ones. This reinforces the essentially uniform observation in all friction work that static friction exceeds dynamic friction, but also illustrates the futility of attempting a more rigorous analysis.

To this point the variation in load on the lower anvil due to the changing mechanical advantage on the slider's weight has been neglected. Having established that Amontons' law is at least a high-fidelity fit for dynamic friction, it becomes possible to correct for this. If friction data are pointwise multiplied by

$$\frac{2P}{2P + (-1.35 \times 10^{-3}x + 5.33 \times 10^{-1})}$$

(where P is the applied load and x is measured in millimetres.) then they become representative of what would have been observed if there were never any contribution from the slider's weight; clearly the impact of this correction is larger for small applied loads. In all cases the effect of the correction is to relatively raise the "tail" of the friction–

displacement traces. Data discussed henceforth have had this correction applied.

Sliding speed has already been noted to correlate positively with friction. The easiest way to investigate this further is to plot coefficient of friction (determined pointwise, as previously explained) against sliding speed; an example graph is shown in Fig. 14. From such graphs it is clear that typical increases of μ with velocity are quite small, usually around 10% of the value at the lowest speed over two orders of magnitude in sliding speed. Additionally, due to the small variation and substantial scatter it is not clear whether what variation does occur is linear or logarithmic with sliding speed. The principal inference that can be drawn from these observations is that viscoelasticity is unlikely to be significant at this interface over any relevant speeds. A more subtle effect like geometric aging (see, for example, Baumberger and Caroli, 2006) of contacts might conceivably explain this modest variation, though the requisite data to make any definite pronouncement are not currently available. It has already been observed that the traces for a given interface bear a strong affinity to each other.

Families of curves corresponding to different sliding speeds at the same load are mathematically similar; that is, simple scaling can bring the details of the traces into coincidence. This is not quite the case for traces corresponding to different loads at the same sliding speed. However, a linear transformation can bring most of the traces corresponding to different loads at most interfaces into good agreement. The linear mapping has two parameters, α and β, and maps the friction force F as

$$F(x) \rightarrow \alpha(F(x) + \beta); \tag{5}$$

note that neither α nor β are functions of x, the displacement. An example of the process of mapping traces onto each other is shown in Fig. 15.

The need for two parameters to describe this transformation suggests two underlying physical friction mechanisms, each corresponding to some proportion of the total friction and varying differently with applied load. Using the transform to bring all of the traces at a given interface into agreement results in a set of α and β values which describe how the mechanisms responsible for friction which varies with displacement (principal friction) and friction which appears unrelated to this (remainder friction), respectively, vary with load.

Since α describes the scaling required to collapse the various traces onto a single trace, α^{-1} describes the way in which the principal friction scales with applied load. Plots of α^{-1} against applied load (an example is shown in Fig. 16) show that (with one exception where neither of the two highest load traces could be fit) the principal friction varies sublinearly with load, in some cases with indices as low as ~0.6; the indices are tabulated for all experiments in Table 4. As is clear from that table, the indices for NW6 are generally higher than for NW1 (no strong statements can be made for NW3 due to poorly fitting traces); and the indices for L8 are higher than for L11, in most cases quite markedly so. All trustworthy indices for principal friction are between 0.57 and 0.86.

Though it clearly is a measure of the amount of remainder friction, there are difficulties in the physical interpretation of

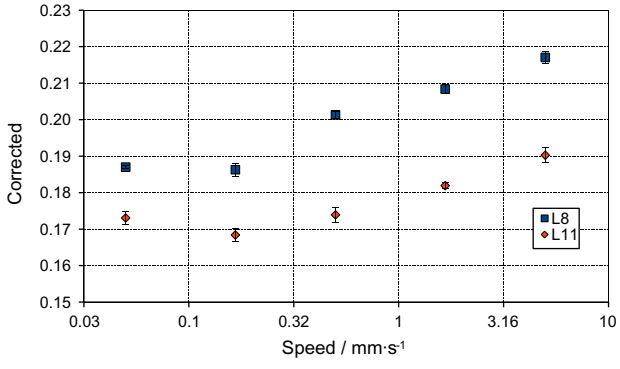

Fig. 14 – An example of variation of coefficient of friction with sliding speed for NW3 and each Lorica Soft slider with the τ and ψ anvils.

a

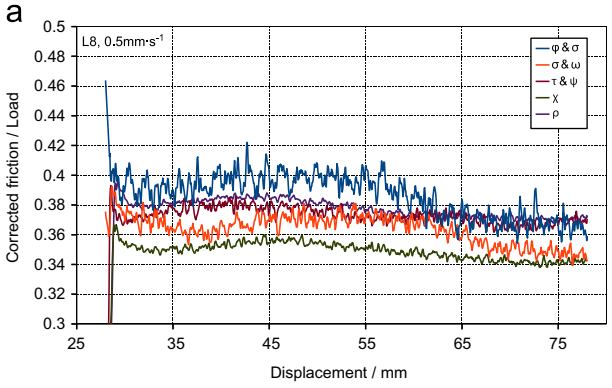

b

Raw load / N	Anvils	α	β
0.25	ϕ & σ	1	0
0.73	σ & ω	—	—
2.65	τ & ψ	0.25	−0.61
8.09	χ	0.08	−1.64
19.01	ρ	0.03	−4.03

c

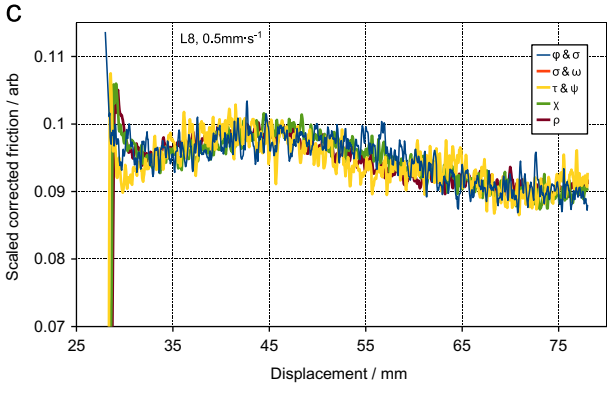

Fig. 15 – The process of mapping friction traces corresponding to different loads at a given interface onto a single master trace. Note the absence of anvils σ and ω from (b) and (c): that trace did not fit. (a) Graph of corrected force against displacement for NW6-L8, sliding at 0.5 mm s^{-1}. (b) Transform parameters for (a). (c) Graph of force against displacement transformed according to the parameters in (b).

β. The nature of the transformation described in Eq. (5) is that if an addition is made to each β value in inverse proportion to the corresponding α value then all of the traces simply move *en bloc*. In consequence, no significance can be attributed to absolute values of β. On the other hand, the change of β with applied load is meaningful. Fig. 17 shows graphs of β against applied load; all but those corresponding to interfaces already identified as problematic are fit well by straight lines. However, the uncertainty in the intercept prevents a direct assessment of the relative magnitudes of the principal and remainder components of friction. Of course, another avenue is open in determining these relative scales: the overall relationship between total friction and load is known to be linear to high precision for each interface, so a simple computational experiment can be run to ascertain the proportions in which a power law with known index but unknown scale (corresponding to principal friction) should be added to a linear function with known gradient but unknown intercept (corresponding to remainder friction) in order to produce a function consistent with experimental results. This is achieved by fitting (least squares) a straight line to the sum of the two contributions, then manipulating first the coefficient of the principal friction term to obtain the correct gradient, and secondly adjusting the intercept of the remainder friction term to obtain the correct overall intercept. The results of this process are shown in Fig. 18; in all cases the coefficient of determination (R^2) is at least 0.998. Though these values reflect a poorer fit than the same straight lines were to the original data, they remain good. It is perhaps not surprising that the fidelity of the fits is reduced: the data have been through several stages of processing before this, and though the fidelity of each has been good, they have inevitably not been perfect. That such agreement between calculated values and experimental fits is possible is strongly suggestive that the approach has merit. Typical proportions of the total friction ascribed to principal and remainder as a function of load are given in Table 5.

Having established the relative scales and manners of variation with applied load of principal and remainder friction for the Lorica Soft-nonwoven interface, it remains to try to identify the mechanisms that they correspond to. This is considered in Section 7, where these data and those from Section 5 are compared.

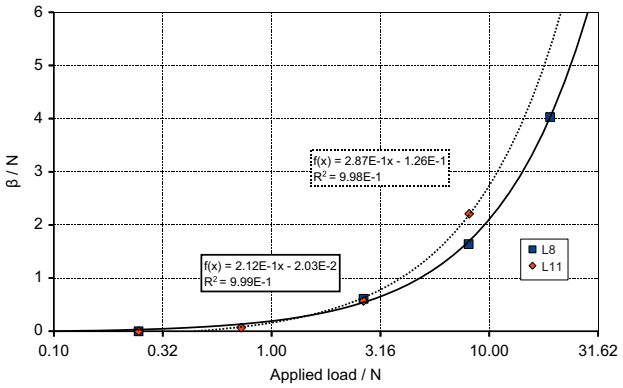

Fig. 17 – An example plot of β against applied load for NW6 sliding against each of the Lorica Soft sliders at 0.5 mm s^{-1}.

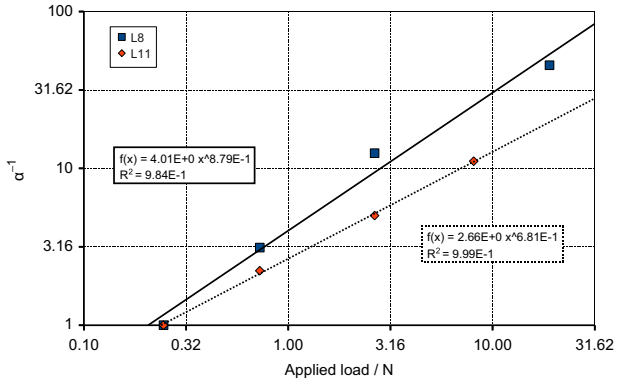

Fig. 16 – An example plot of α^{-1} against applied load for NW1 against each Lorica Soft slider, sliding at 0.5 mm s^{-1}.

Table 4 – The scaling factor (α^{-1}) for principal friction has been found to vary as a power law with applied load. The indices for each of the tested interfaces and sliding speeds are shown in the table.

Nonwoven	Slider	Speed (mm s^{-1})	α^{-1} index
NW6	L8	0.05	0.797
		0.167	0.862
		0.5	0.789
		1.67	0.753
		5	0.761
	L11	0.5	0.568
NW3	L8	0.5	1.08[a]
	L11	0.5	0.554[a]
NW1	L8	0.5	0.879[a]
	L11	0.5	0.681

[a] Indicates that something was wrong with the data which might make these numbers unreliable.

7. Summary and conclusion

A brief summary of the main results presented will be given before making connections between the two distinct experiments. Section 5 found that the contact length of fibres constituting the interface between nonwoven and skin (surrogate) varied logarithmically with load, increasing by a factor of two to three (depending on the nonwoven) over two orders of magnitude of load. Assuming that the cylindrical fibres pressing into the skin (surrogate) obeyed Hertzian contact mechanics, predictions were made on the basis of the experimental data for the variation of adhesive friction (assuming no roughness on the scale of fibres) and viscoelastic friction (based on the Greenwood and Tabor model, 1958) with load. Power law fits were good for both quantities; subject to their assumptions, adhesive friction was predicted to vary as $P^{0.6}$ and viscoelastic friction as $P^{1.4}$, with slight variations between nonwovens. NW1 had the highest contact fraction, followed by NW6, and then NW3. NW6 had the highest viscoelastic loss, followed by NW3, and finally NW1; however, this ranking is a little uncertain as

Lorica Soft's loss factor may not be the same for all fibre diameters.

In Section 6 it was found that for Lorica Soft against each of the nonwovens overall friction against load could be well fit by a straight line, though there was a hint of sublinearity, especially at low loads. There was good evidence that the friction was composed of two different components (termed principal and remainder), the former varying with load sublinearly with a typical index around 0.75, and the latter varying linearly with load. Friction did generally increase with velocity, but only by about 10% over two orders of magnitude velocity change; it was not possible to ascertain the manner of variation. Finally, under equivalent conditions NW1 had the highest friction, followed by NW3, and finally NW6.

Comparing the contact measurement and friction data obtained in this work, it is reasonable to conjecture that the principal friction is due to "nearly smooth" adhesion; that is, where the assumption that the skin and nonwoven fibres are smooth on the scale of a fibre diameter nearly holds. This is supported by the index of variation of principal friction with load only slightly exceeding the index found in Section 5.5 for contact fraction. According to the work of Archard (1953, 1957) and others, roughness has the effect of increasing such indices towards unity; the slight difference in indices is thus attributed to slight roughness. Unfortunately, though this identification is quite plausible there is no direct evidence to support it.

Only two mechanisms are known which give rise to the linear relationship between friction and load that remainder friction demonstrates: plastic junction formation (following Bowden and Tabor, 1986); and adhesion at rough, elastically deforming junctions (Archard, 1953, 1957 and others). The former is inconsistent with the lack of observed damage, apparently implicating the latter. This would suggest that Lorica Soft-nonwoven friction was all due to adhesion and (after a wear-in period) elastic deformation, but that two distinct populations of contacts took part: those corresponding to principal friction forming a fairly smooth interface; those corresponding to remainder friction forming a rough one. The lack of an explicitly viscoelastic friction mechanism is certainly consistent with the very limited variation of friction with sliding speed; what variation there is can perhaps be attributed to a rather more subtle viscoelastic effect like geometric aging.

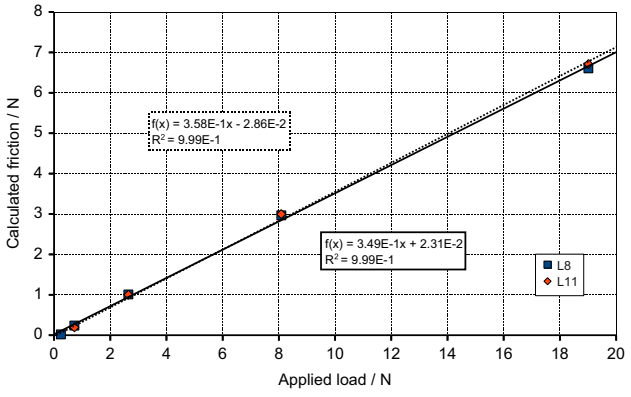

Fig. 18 – An example graph of calculated friction against load, comparing the models with the original linear fits from the data.

The primary purpose of the work described here was to use the relatively simple nonwoven-Lorica Soft system to develop experimental and interpretative methodologies that could be used in future studies of friction between nonwovens and skin, and this has been achieved. Measurements with the model system proved robust enough to provide insights into friction mechanisms, giving confidence that a similar approach with nonwoven and excised skin should be fruitful, if more challenging practically.

By the arguments outlined in Section 5.1, the results on variation of contact area with load for the nonwoven-Lorica Soft interface could be transferred to the same nonwoven against skin simply by changing the mechanical properties used in the final calculations, though it should be remembered that the absolute values provided by this calculation do not allow for surface relief. However, although it is likely that structurally similar nonwovens will behave similarly and show similar variation of contact area with load, the results cannot be applied to substantially different materials; a new run of experiments would be required for them.

The friction force results and subsequent analysis are not portable to skin from Lorica Soft on the strength of the currently know relationship between them, though the methods could be expected to be effective if skin were used. In particular, the division of friction into principal and remainder may or not may apply if skin were used. An interesting avenue for future work would be to establish whether this division is more general. If this were the case and the features and properties responsible for each could be identified then experimental results may become transferable between different though qualitatively similar interfaces.

Table 5 – Approximate breakdown of friction into principal and remainder parts. It must be emphasised that these numbers are approximate indicators, averaging across interfaces and sliding speeds. In general, reducing the sliding speed relatively increases the importance of the remainder. At low loads the remainder component is negative; whilst clearly unphysical this is simply because the offset is attributed entirely to this term.

Anvils	Load (N)	Remainder (N)	Principal (N)
ϕ and σ	0.25	−0.15	0.12
σ and ω	0.73	−0.05	0.25
τ and ψ	2.65	0.30	0.70
χ	8.09	1.6	1.5
ρ	19.01	4	3

Acknowledgments

We acknowledge with thanks SCA Hygiene Products AB and the Engineering and Physical Sciences Research Council for funding the work.

Appendix A. The production of anvils for applying uniform normal stress at nonwoven-Lorica Soft interfaces

The key to producing appropriate anvils is to turn the problem on its head: instead of trying to produce the shape that gives rise to a set of forces, apply the set of forces and take note of the shape. Further, given the complex materials involved, it is far easier to use the materials and configurations themselves than to try to imitate them. Following these principles, the equipment illustrated in Fig. A.1 was built to implement the correct force fields.

The apparatus provides a known, constant normal stress against the test surface via fluid pressure; applies a corresponding shear stress by pulling a strip of nonwoven between the retaining membrane and the aforementioned surface (Fig. A.2); and measures the normal force with a balance. The equipment is built upon a balance: the test surface (along with necessary spacers) is fixed to the balance pan; the remainder of the equipment rests upon the balance surround. Pressure chambers were made by cutting down a 50 ml, 26.5 mm syringe are. The open end of the syringe is covered with a latex membrane held in place by a wide rubber band.

Anvils are cast with a three-stage process. The first stage involves introducing a small quantity of a fast-curing resin (polyurethane (PUR), Axson F16, Axson UK, Newmarket, UK) into the syringe before pressurising it, applying pressure, and removing the cast shape once the resin has cured (typically around ten minutes). The second stage involves stretching smooth latex rubber over the blank and producing a counter-cast. Finally, a high-optical-quality anvil is cast in slow-curing epoxy using the counter-cast as a mould.

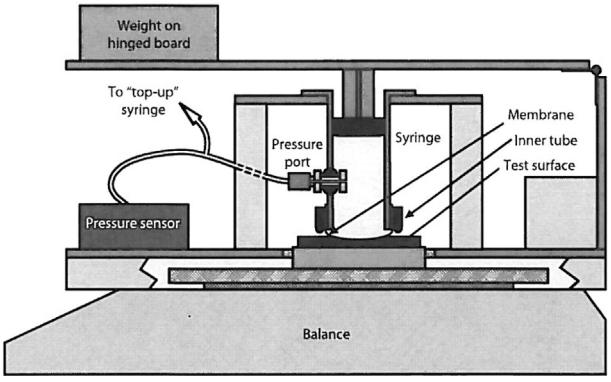

Fig. A.1 – The apparatus used to produce uniform-stress anvil shapes. The equipment is built onto a balance; part of one side has been cut away for visual clarity.

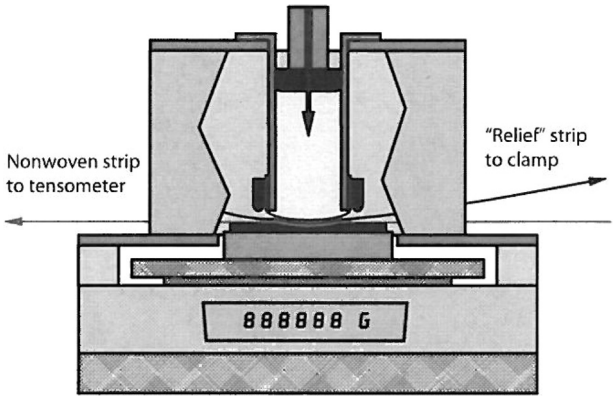

Fig. A.2 – The shear force required to obtain the correct anvil shape is provided by a nonwoven strip pulled along at a constant rate by the tensometer used in all other experiments. In order to prevent the membrane from shearing unduly a "relief strip" is also included which pulls in the opposite direction and is pre-tensioned before sliding begins.

REFERENCES

Ajayi, J.O., 1992. Effects of fabric structure on frictional properties. Textile Research Journal 62, 87–93.

Archard, J.F., 1953. Contact and rubbing of flat surfaces. Journal of Applied Physics 24, 981–988.

Archard, J.F., 1957. Elastic deformation and the laws of friction. Proceedings of Royal Society of London Series A 243, 190–205.

Baumberger, T., Caroli, C., 2006. Solid friction from stick-slip down to pinning and aging. Advances in Physics 55, 279–348.

Bobjer, O., et al., 1993. Friction between hand and handle. Effects of oil and lard on textured and non-textured surfaces; perception of discomfort. Applied Ergonomics 24, 190–202.

Bowden, F., Tabor, D., 1986. The Friction and Lubrication of Solids. OUP, Oxford, UK (Chapter 5).

Comaish, S., Bottoms, E., 1971. The skin and friction: deviations from Amontons' laws, and the effects of hydration and lubrication. British Journal of Dermatology 84, 37–43.

Cottenden, D.J., 2011. A Multiscale Analysis of Frictional Interaction Between Human Skin and Nonwoven Fabrics, Table 2.1 and Associated Text. Ph.D. Thesis, University College London, London, UK. ⟨http://discovery.ucl.ac.uk/1301772/⟩.

Cottenden, A.M., Wong, W.K.R., Cottenden, D.J., Farbrot, A., 2008. Development and validation of a new method for measuring friction between skin and nonwoven materials. Journal of Engineering in Medicine 222, 791–803.

Derler, S., Schrade, U., Gerhardt, L.-C., 2007. Tribology of human skin and mechanical skin equivalents in contact with textiles. Wear 263, 1112–1116.

El-Shimi, A., 1977. In vivo skin friction measurements. Journal of Society of Cosmetic Chemists 28, 37–51.

Ferguson-Pell, M.W., Bell, F., Evans, J.H., 1976. Interface pressure sensors: existing devices, their suitability and limitations. In: Kenedi, R.M., Cowden, J.M., Scales, J.T. (Eds.), Bedsore Biomechanics. Macmillan, London, UK (Chapter 5).

Gerhardt, L.-C., Strässle, V., Lenz, A., Spencer, N.D., Derler, S., 2008. Influence of epidermal hydration on the friction of human skin against textiles. Journal of Royal Society Interface 5, 1317–1328.

Gerhardt, L.-C., Lenz, A., Spencer, N.D., Münzer, T., Derler, S., 2009. Skin-textile friction and skin elasticity in young and aged persons. Skin Research & Technology 15, 288–298.

Greenwood, J., Tabor, D., 1958. The friction of hard sliders on lubricated rubber: the importance of deformation losses. Proc. Phys. Soc. Proceedings of the Physical Society 71, 989–1001.
Gwosdow, A.R., Stevens, J.C., Berglund, L.G., Stolwijk, J.A.J., 1986. Skin friction and fabric sensation in neutral and warm environments. Textile Research Journal 56, 574–580.
Hendriks, C.P., Franklin, S.E., 2010. Influence of surface roughness, material and climate conditions on the friction of human skin. Tribology Letters 37, 361–373.
Hong, K.H., Kim, S.C., Kang, T.J., Oh, K.W., 2005. Effect of abrasion and absorbed water on the handle of nonwovens. Textile Research Journal 75, 544–550.
Hosseini Ravandi, S.A., Toriumi, K., Matsumoto, Y., 1994. Spectral analysis of the stick-slip motion of dynamic friction in the fabric surface. Textile Research Journal 64, 224–229.
Jeddi, A.A.A., Shams, S., Nosraty, H., Sarsharzadeh, A., 2003. Relations between fabric structure and friction. Part I. Woven fabrics. Journal of the Textile Institute 94, 223–234.
Johnson, K., 1985a. Contact Mechanics, vol. 59. CUP, Cambridge, UK.
Johnson, K., 1985b. Contact Mechanics, vol. 47. CUP, Cambridge, UK.
Johnson, K., 1985c. Contact Mechanics, vol. 49. CUP, Cambridge, UK.
Johnson, K., 1985d. Contact Mechanics, vol. 101. CUP, Cambridge, UK.
Kaye, G.W.C., Laby, T.H., 2004. Tables of Physical and Chemical Constants. ⟨http://www.kayelaby.npl.co.uk/⟩. (accessed 16.04.10).
Kenins, P., 1994. Influence of fiber type and moisture on measured fabric-to-skin friction. Textile Research Journal 64, 722–728.
Nakajima, K., Narasaka, H., 1993. Evaluation of skin surface associated with morphology and coefficient of friction. International Journal of Cosmetic Science 15, 135–151.
Park, A.C., Baddiel, C.B., 1972. Rheology of stratum corneum. I. A molecular interpretation of the stress–strain curve. J. Soc. Cosmet. Chem. Journal of the Society of Cosmetic Chemists 23, 3–12.
Ramkumar, S.S., Roedel, C., 2003. Study of needle penetration speeds on frictional properties of nonwoven webs: a new approach. Journal of Applied Polymer Science 89, 3626–3631.
Wang, X.Y., Gong, R.H., Dong, Z., Porat, I., 2006. Frictional properties of thermally bonded 3d nonwoven fabrics prepared from polypropylene/polyester bicomponent staple fibre. Polymer and Engineering Science 46, 853–863.
Zhang, M., Mak, A.F.T., 1999. *In vivo* friction properties of human skin. Prosthetics and Orthotics International 23, 135–141.